Journal of Materials Chemistry A

ROYAL SOCIETY OF CHEMISTRY

PAPER

View Article Online
View Journal | View Issue

Cite this: J. Mater. Chem. A, 2025, 13, 3894

Calix[4]arene@MIL-101 as host@MOF for cage-in-cage pore space partitioning for enhanced CO_2 separation and catalysis†

Saied Shafiei Navid, [ab] Rahman Hosseinzadeh, *[a] Robert Oestreich, [b] Soheil Abdpour,[b] Thi Hai Yen Beglau[b] and Christoph Janiak *[b]

Highly stable *para*-sulfonated calix[4]arene (SCA), a bowl-shaped macrocycle possessing intrinsic porosity, was incorporated into the spherical voids of the micro–mesoporous MIL-101(Cr) metal–organic framework by adsorptive loading from a solution. The pore-space partitioning in the MOF by polar functionalized macrocyclic molecules, which can also act as hosts, led to the host@MOF composite SCA@MIL-101 which demonstrated a high affinity to CO_2 without the involvement of alkaline amino functionalities. The SCA@MIL-101-*w* materials with $w = 5$, 10 and 30 wt% SCA showed high stability (including in aqueous medium, at least under non-basic conditions), and slow leaching kinetics due to the near match of the SCA size and the pore entrances of the MOF. Despite the lower surface area and pore volume for $w = 30$ wt% SCA in MIL-101 ($S_{BET} = 1073$ m^2 g^{-1} and $V_{pore} = 0.52$ cm^3 g^{-1}) *vs.* MIL-101 (2660 m^2 g^{-1} and 1.0 cm^3 g^{-1}), the pore-space partitioning approach allows the improvement of the CO_2 uptake capacity to 103 cm^3 g^{-1} for SCA@MIL-101-30 over MIL-101 with 66 cm^3 g^{-1} (273 K and 1 bar). This also increases the CO_2/N_2 selectivity, such that SCA@MIL-101-30 has a selectivity of 11 *vs.* 4 for MIL-101 for a 15 : 85 v : v CO_2/N_2 mixture at 293 K and 1 bar. Additionally, the SCA@MIL-101-30 composite showed good catalytic activity in the esterification of carboxylic acids, giving quantitative conversion on par with H_2SO_4 under the chosen conditions.

Received 15th October 2024
Accepted 19th December 2024

DOI: 10.1039/d4ta07357f

rsc.li/materials-a

1. Introduction

Advanced microporous materials for the adsorption and separation of small molecules, particularly gases, have attracted considerable interest in recent years.[1,2] The more recent metal–organic frameworks (MOFs) and covalent organic frameworks (COFs) offer higher surface areas and better tuneability in general compared to traditional zeolites and active carbons.[3,4] The interaction between the adsorbent and adsorbate is strongly enhanced under the conditions of respective host and guest complementarity, while the overall optimum interactions require uniformity of the pore sizes, *i.e.* periodicity/crystallinity. The tuneable and crystalline MOFs with record-holding surface areas have the potential to demonstrate optimal affinity for a broad range of small-molecule adsorbates.[5] However, there is a practical limit to ligand-site modification, particularly, if applications are considered.[6,7] In other words, the preparation of the majority of potentially feasible MOFs is prohibitively expensive. An alternative way to synthesizing custom-tuned MOFs is the modification of existing high-quality MOFs using 'pore space partition' *via* the introduction of suitably functionalized species.[8,9] In rare but important cases, such modification is carried out during the synthesis of the MOF *via* adding a multi-topic anchoring co-ligand, which binds to the available non-saturated metal sites, thereby partitioning the pore (*e.g.* in the case of the pacs platform with partitioning of the MIL-88 pore space).[10] The latter method demands a near perfect MOF-species match and is better applicable when one of the components, particularly the MOF, is flexible. A more easily achievable and more general possibility is the introduction of large (semi-)rigid molecules, such as macrocycles or molecular cages with an accessible inner part (*i.e.*, possessing intrinsic porosity), which could provide additional characteristics regarding the affinity towards adsorbates.[11,12]

The uniqueness of the MIL-101(Cr) (denoted as MIL-101) MOF as a porous host is in the combination of high robustness, high surface area, and large pore sizes (Scheme 1a, b and Fig. 1). The two constituting cavity types have approx. ~3.4 and 2.9 nm inner diameters,[13] *i.e.*, allow the incorporation of guests with such sizes, which renders MIL-101 one of the rare representatives of stable micro–mesoporous MOFs (the limit between micro- and mesopores is set by definition at 2.0 nm).

[a]Department of Organic Chemistry, Faculty of Chemistry, University of Mazandaran, Babolsar, Iran. E-mail: r.hosseinzadeh@umz.ac.ir

[b]Institut für Anorganische Chemie und Strukturchemie, Heinrich-Heine-Universität Düsseldorf, 40225 Düsseldorf, Germany. E-mail: janiak@hhu.de

† Electronic supplementary information (ESI) available: Materials, instruments, synthesis, NMR results and gas sorption graphs. See DOI: https://doi.org/10.1039/d4ta07357f

Such large pores allow the incorporation of species with a significant molecular size, including various functionalities, which might be too large for typical MOFs (*e.g.*, macrocycles with chelating capabilities).[14]

There are a number of large (semi-)rigid macrocyclic and (open) cage molecules (jointly abbreviated as CMs in this work), *e.g.*, cyclodextrins, cryptands (and crown-ethers to some extent), cucurbiturils, and calixarenes. Their cavities could reach more than 3 Å, which is enough for the tight binding of small gas molecules or, if desired, a special guest (particularly metal ions), provided that a donor group is present. The functionalized single-atom thick walls of CMs provide an ample surface for optimal pore space partitioning.[15–17] The potential of CMs for adsorption is immediately apparent, but with very few exceptions, they are rarely viewed as individual adsorbent materials since their intrinsic porosity is usually inaccessible due to their tightly packed crystalline state.[18] However, the unique properties of CMs (high specific surface area of an isolated molecule, polar sites, potential functionalizability and added features desirable for applications, such as catalysis) make them interesting candidates as additional or secondary host species in intrinsically porous primary host structures.[2,12,19–23]

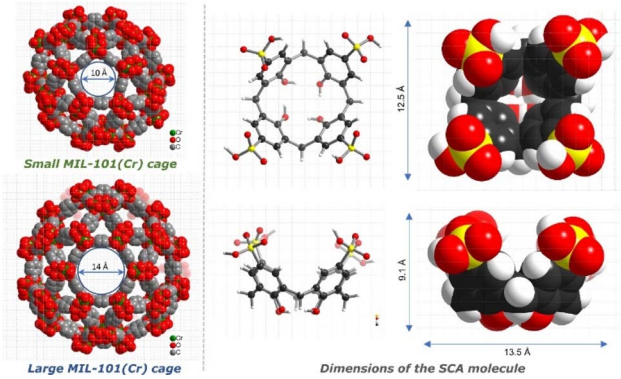

Fig. 1 Left: Space-filling model representation of the MIL-101 cages featuring the projections of the respective pentagonal and hexagonal pores, shown on a 1 × 1 Å stepped grid. Right: The molecular dimensions of the semi-flexible SCA molecule (the crystal structure of SCA with a CSD FEBTAI code was used). Note the slight deflection of the structure's geometry from the one with the highest symmetry, which is caused by intermolecular interactions in the crystal structure.

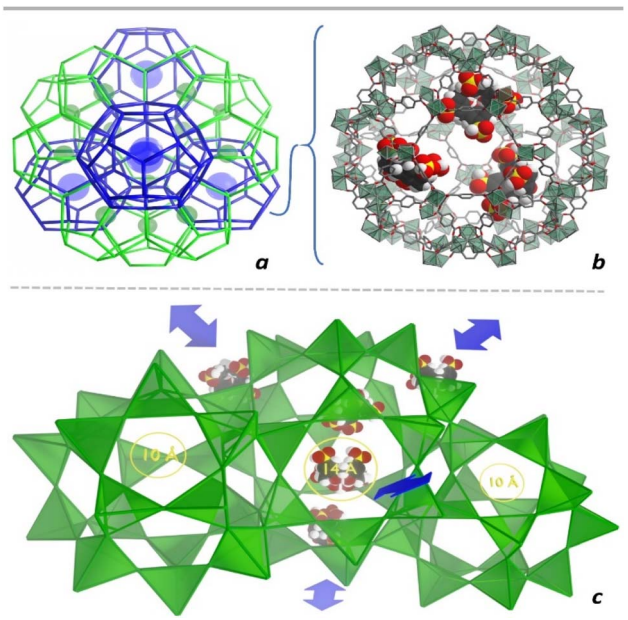

Scheme 1 CM@framework composites with the example of SCA@-MIL-101, reported in this work. (a) Topological representation of the MIL-101 framework structure with a **mtn** topology, where the nodes represent supertetrahedra with vertices corresponding to trinuclear $\{Cr_3O(OH)(H_2O)_2(O_2C-)_6\}$ secondary building units (SBUs).[13] The pore-system is constituted by large pore-cavities with hexagonal and pentagonal pore entrances as well as small dodecahedral cavities with pentagonal-only pore entrances, while the stoichiometry of the large and small cavities is 1 : 2. The edges of the large cavities are shown in blue, the remaining edges in green, the centers of the large and small cavities are marked using blue and green spheres respectively. Importantly, the two pore-types form contiguous 3D pore-subsystems, while the large pore subsystems are connected by only large hexagonal windows. The vdW entrance window of the latter is the limiting size for a guest, which could enter the pores. (b) The large cage of the MIL-101 structure, depicted at the molecular level, with the SCA molecules (the space-filling model used for the SCA molecules precisely reflects the vdW sizes relative to the size of the framework). (c) The model of the MIL-101 framework at the level of the supertetrahedra with the expected pathways of diffusion of the SCA molecule only *via* the larger hexagonal pores.

The non-bonded incorporation of CMs into a porous framework – in the form of a 'CM@framework' or here as a host@MOF composite[23] (Scheme 1a and b) – offers the possibility to utilize special adsorptive properties of the CM molecules as hosts by enabling access for small adsorbate molecules (*cf.* with the incorporation of CMs in flexible organic polymers, where little or no access is guaranteed).[24–26] Such incorporation is a simplified alternative to modification by grafting CMs to the walls of the pores, as the latter way demands additional prerequisites for binding. The incorporated CMs could be contraposed to CM-aggregates, associated *via* hydrogen- or coordination bonds with typical drawbacks of too tight association, lability, low specific surface areas and poor access for adsorbate molecules.[27]

Besides pore partitioning[10] and the host@MOF concept[23] the incorporation of CMs into the MOF pores can also be discussed as a confinement effect.[28,29] The chemical confinement of a molecule inside another larger molecule, here a CM inside a MOF will change the electron density and chemical reactivity of the CM.[28] For enhanced CO_2 capture in MOFs, the chemical confinement of pre-adsorbed polar (water, alcohols, and amines) and non-polar (toluene and benzene) molecules was employed.[29] The confinement effect may lead to physical–chemical interactions involving both the confined species and the MOF and create, *e.g.*, an additional bottleneck effect, but most importantly, here it should make the intrinsic porosity of the CM accessible which is often not available in its neat solid state. Furthermore, the confinement effect will lead to extrinsic pores between the CM and the pore walls of the MOF for further interactions of the guest molecules and possibly also for selective mass transfer pathways through interaction adsorption or repulsion effects.[23]

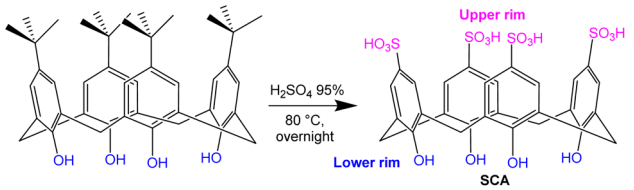

Scheme 2 The synthesis of SCA from *p*-*tert*-butyl-calix[4]arene.

Calix[*n*]arenes ($n = 4$–8; see Scheme 2a for an example with $n = 4$) are distinguished among other CMs by their high chemical stability (matching or even exceeding those of the polyether macrocycles) and, more importantly, they could be relatively easily functionalized at both the 'upper-' and 'lower' rims (*O*-functionalization of the phenols in the latter case, which could be performed under mild conditions).[30] The non-functionalized lower rim with phenolic groups has a high affinity towards metal ions due to efficient coulombic interaction-enhanced chelation, which is somewhat akin to affinity expressed by crown-ethers/cryptands but merely *via* charge neutral complexation.[31,32] The chemical stability of the calixarene core allows the introduction of various active functionalities.[33]

Para-sulfonated calix[4]arene (SCA, see Scheme 2b), is a semi-rigid bowl-shaped macrocyclic molecule with an accessible inner part. The cavity is hydrophobic at the medium segment of the bowl-shaped molecule, while hydrophilic at both the upper and lower rims due to the respective functionalization with the –OH and $–SO_3H$ groups. The enhanced set of polar groups in the SCA molecule is expected to have an increased affinity for polarizable molecules such as CO_2 compared to non-sulfonated analogues. The combination of "polar" interactions, including the ones involving H-bonds, ensured by the presence of SO_3H and OH groups, as well as the low-polar interaction with the medium part of the rim, including possible π···π stacking and C–H···π interactions, renders the SCA molecule a versatile adsorbent. SCA could also impart water solubility and has been used as a homogeneous Brønsted catalyst, for dye removal, as a backbone for dendrimers, and as an organic modifier in nanocomposites.[34–37]

In this work, we explore the possibility of incorporating the smallest and the most rigid calix[4]arene in the form of the tetrasulfonic acid (SCA), into the pores of MIL-101.[38] In a broader context, the aim is the incorporation of a highly chemically stable, post-synthetically modifiable calixarene-platform (it could be viewed as a further step compared to the CB6@MIL-101 material, with the chemically less stable and not modifiable cucurbituril, published by us recently).[22] The novel SCA@MIL-101 is tested in the context of selective CO_2 adsorption in a mixture with N_2 or CH_4 and Brønsted catalytic activity towards esterification.

2. Materials, instruments, and methods

All the starting materials were purchased from commercial suppliers and used as obtained without further purification and also all the instruments and methods are listed in the ESI.†

3. Synthesis and analytics

3.1. Synthesis of SCA

Scheme 2 shows the synthesis route of *p*-sulfonated-calix[4]arene (SCA) based on the method which was reported by Tauran *et al.* (see the ESI†).[39]

3.2. Synthesis of MIL-101

MIL-101 was synthesized on a gram scale by using chromium(III) nitrate nonahydrate and benzene-1,4-dicarboxylic acid with a procedure published by us earlier (see the ESI†).[40]

3.3. Synthesis of the SCA@MIL-101-*w* composites

A standard procedure was used, as follows. A specified amount of SCA was fully dissolved in 2 mL of D_2O and the solution was added to 10 mg of activated MIL-101 (D_2O was used because of the subsequent SCA quantification in the centrifugate). After equilibration overnight with shaking, the mixture was centrifuged and the supernatant was separated. The obtained material was washed two times using 3 × 2 mL of deionized water and 2 × 2 mL of ethanol for 6 hours. Finally, the obtained composite was activated at 150 °C for 12 h under dynamic vacuum (10×10^{-2} Torr). The SCA@MIL-101 prepared with different loadings (w) of SCA is denoted thereafter as SCA@MIL-101-w with $w = 5$, 10, or 30, according to the initial amount of SCA in mg. The amount of SCA loading could be performed reproducibly and the SCA loading was post-synthetically determined by CHNS elemental analysis together with quantitative ^{1}H NMR analysis of the supernatant and digested SCA@MIL-101 (see Tables S1 and S2† for details). For larger scale synthesis, the reaction was repeated with a 10-fold amount of SCA and 50 mg of activated MIL-101. The yields of SCA@MIL-101-w are given in Table 1.

4. Results and discussion

There is an evident dichotomy of possibilities for incorporating a guest into a porous framework. These are the adsorptive loading of a guest and the construction of the framework around the guest *in situ* (the latter approach is sometimes called the 'bottle-around-the-ship' method, changing the standard expression to underpin that the framework is formed around the guest). While the latter method potentially allows the

Table 1 The yields of the prepared composites with different amounts of SCA

Sample	MIL-101[a] (mg)	SCA[a,b] (mg)	Yield[a,c] (mg)
SCA@MIL-101-5	10/50	5/50	13.1/128.4
SCA@MIL-101-10	10/50	10/100	15.3/150.7
SCA@MIL-101-25	10/50	25/250	18.7/184.8
SCA@MIL-101-30	10/50	30/300	19.6/192.5

[a] first value corresponds to small-scale synthesis, and the second value to large-scale synthesis. [b] The amount of the SCA used during the adsorptive loading (*i.e.*, the initial amount added). [c] The amounts are given after activation.

irreversible encapsulation of the guest, which is beneficial for applications, the process is poorly controlled and the purity, as well as structural uniformity, of the product is questionable. While the adsorptive loading does not ensure irreversible encapsulation, it yields uniform well-"equilibrated" composites crucial to ensuring optimal qualities, particularly regarding porosity. Our previous work with the adsorptive loading of cucurbit[6]uril demonstrated the viability of the incorporation of macrocyclic molecules for the modulation of adsorption properties.

Calixarenes were purposefully chosen as more stable and modifiable macrocyclic molecules compared to cucurbiturils. The size of the used SCA is ~13 × 13 × 9 Å (Fig. 1-left), which is very close to the size of the large hexagonal window of MIL-101 with a diameter of ~14 Å vdW according to a conservative estimation (Fig. 1-right). While local molecular motion ensures somewhat larger effective pore sizes than the above estimates from structural data, the possibility of the entrance of the SCA molecules in the smaller cages of MIL-101 with ~1.0 nm vdW pore window opening was viewed as improbable during the initial planning of the work. The closeness of the SCA molecular size and the MIL-101 largest pore entrance size should ensure a kinetically hindered desorption, amplified by the hydrophilic interactions between the $-SO_3H$ groups of SCA with the hydrophilic metal clusters of MIL-101.

The adsorptive loading was performed using an SCA solution in D_2O. Specified amounts of the activated MIL-101 and a defined volume of an SCA solution with a known concentration were shaken overnight for equilibration. The incorporated SCA amount was established using CHNS analysis and ^{1}H NMR spectroscopy of the supernatant and the decomposed composites (see the ESI for details, Tables S1 and S2†).

A leaching experiment which was performed for SCA@MIL-101-30 showed nearly no SCA-related signal in the ^{1}H NMR spectrum of the washing solution, which means that the desorption/leaching is minimal (see the ESI for details, Fig. S6†). The observation of such a high affinity is somewhat surprising, but it seems that due to the relatively large size of the SCA molecules and the multiple π···π and C–H···π interactions, the desorption of SCA molecules from the pores is very slow.

The successful incorporation of SCA molecules into MIL-101 was further supported by the FT-IR spectra of the resultant SCA@MIL-101 composites (Fig. 2a) with the SCA bands at 3411, 1218, 1041, and 627 cm^{-1} respectively. Unfortunately, the strongest SCA-related bands are at least partially coinciding with the strong bands associated with MIL-101. Hence, the increase of the SCA-related intensities with the increase of the amount of the incorporated SCA is weakly expressed. However, there are subtle SCA-related shifts, which are nearly SCA-content independent, reflecting the relatively uniform interactions between SCA and MIL-101. The PXRD patterns of the SCA@MIL-101 composites are close to those of the neat MIL-101 (Fig. 2b), demonstrating the preservation of the crystallinity during the incorporation. As expected, the peaks have slightly different relative intensities, particularly evident at low angles, which is attributed to the increased incorporation of the

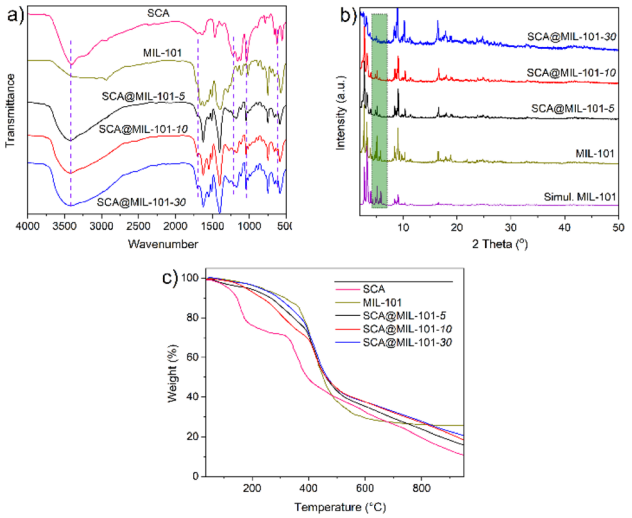

Fig. 2 (a) FT-IR spectra of SCA, MIL-101 and SCA@MIL-101-w composites, (b) PXRD patterns of SCA@MIL-101 composites, experimental and simulated MIL-101 (simulated from the deposited cif file under CCDC/CSD-605510), and (c) TGA curves of SCA, MIL-101 and SCA@MIL-101-*w* (*w* = 5, 10, 30) composites under a nitrogen atmosphere (heating rate 10 °C min^{-1}).

SCA molecules into the pores (the observation of these differences in the PXRD indicates that the distribution is not completely random and a certain ordering is present). The absence of clearly identifiable additional peaks, which would be associated with a neat SCA phase crystallized outside of the pores, reflects the crystalline phase purity of the composite.

The thermogravimetric analysis (TGA) under a N_2 atmosphere showed that the SCA@MIL-101 composites are stable up to ~200 °C. Further increase in the temperature causes gradual decomposition (the lower stability compared to MIL-101 is expected due to the significant SCA acidity). With the increase in the incorporated SCA content, the relative amounts of the carbonized residues were also decreased, as expected (Fig. 2c). Two major mass loss steps could be distinguished in the TGA curves of MIL-101 and SCA@MIL-101-*w* (*w* = 5, 10, 30) composites with only a slight variation. The first mass loss step in the 30–250 °C range (7 wt%) is associated with a loss of water, both physisorbed water and the coordinated aqua ligands of the $\{Cr_3O(OH)(H_2O)_2(O_2C–)_6\}$ SBU. It is possible that the presence of the hydrophilic SCA slightly modulates the dehydration profile. The second mass loss step at 275–400 °C (~60 wt%), is primarily associated with the decomposition of both the framework and the SCA molecules.[41] The mass loss associated solely with the decomposition of SCA starts at ~330 °C. It is also weakly discernible on the TGA curves of the composites upon comparison with the TGA curve of the neat SCA. The first step in the TGA of SCA up to ~180 °C is associated with the loss of adsorbed water. It is interesting to note that despite the acidity of the SCA, the onset of the decomposition temperature for the MIL-101 framework of the composites did not change significantly (which does not preclude an earlier structural collapse). The TGA data cannot provide reliable information about the

SCA wt% in the composites due to somewhat different amounts of adsorbed water and no sharp definition of the weight loss steps.

Scanning electron microscopy (SEM) images of MIL-101 and SCA@MIL-101 materials indicate that the morphology of the MIL-101 microcrystals is preserved after the formation of the composites, *i.e.*, after the incorporation of the SCA molecules (Fig. S7†). The EDX elemental mapping analysis confirmed the even distribution of the sulfur associated with the SCA, throughout the composite particles (Fig. S8†).

5. N_2, CO_2, and CH_4 gas adsorption, heats of adsorption and selectivities

The porosity characteristics of the synthesized materials were established using N_2 adsorption isotherms at 77 K (Fig. 3a and S9†). Interestingly, for the as-isolated microcrystalline SCA, a low but detectable surface area of 41 m^2 g^{-1} was found reflecting the at least partial accessibility of the residual free volume, associated with non-tight packing of the bowl-shaped macrocyclic molecules. MIL-101 and the derived composites showed IUPAC Type Ib isotherms12 consistent with the presence of both micro- (<2 nm diameter) and mesopores (2–50 nm), associated with the pentagonal and hexagonal entrance pore-windows on the one hand and both the large and small pore cavities on the other hand. For MIL-101 and the MIL-101-*w* materials, where $w = 5$, 10, and 30, BET surface areas of 2658, 2156, 1497, and 1073 m^2 g^{-1}, respectively, were found (Table S5†), which is consistent with pore occupation and blocking through the increase of SCA loading. Still, even the SCA@MIL-101-30 with a loading supposed to be near saturation levels, had a very significant BET surface area of 1073 m^2 g^{-1} and a total pore volume of around 0.52 cm^3 g^{-1} (from NLDFT). The latter observation indirectly corroborates the assumption that the smaller dodecahedral cages with the narrower pentagonal pore openings might not readily adsorb the relatively large SCA molecules.

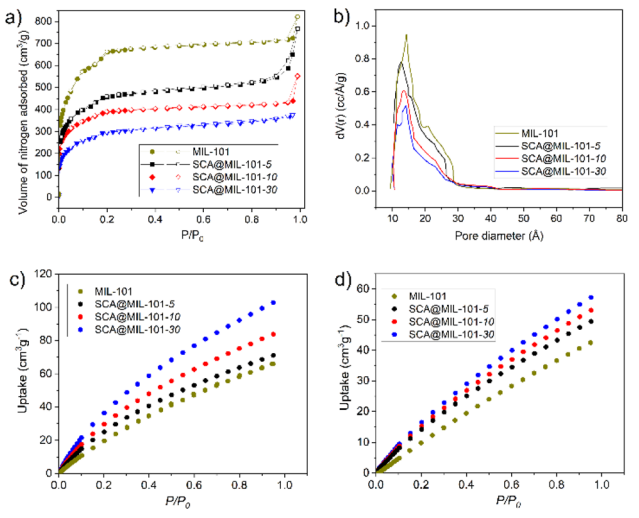

Fig. 3 (a) N_2 sorption isotherms of MIL-101 and the derived SCA@MIL-101 composites at 77 K, (b) pore size distribution of MIL-101 and all composites, (c) and (d) CO_2 adsorption isotherms of SCA@MIL-101-*w* ($w = 5$, 10, 30), and MIL-101 measured up to 1 bar at 273 K and 293 K. For clarity, only the adsorption part of the isotherm is given here; see Fig. S11 and S12† for both the adsorption and desorption branches.

The pore volume distribution and cumulative pore volume estimated by DFT calculations are given in Fig. 3b and S10,† respectively. The characteristic bimodal pore-size distribution of MIL-101 is generally retained in the composites, but the contribution of the large pores, associated with the larger cages decreases strongly in the composites following the increase in the SCA loading. These results reflect the pore space partitioning by the SCA molecules. The partitioning aims at enhancing gas adsorption characteristics by optimizing the sizes of the adsorbate molecules and the pores. An optimum pore size for a linear gas molecule with a length L_{ads} exists in an adsorbent structure with opposite surfaces at a distance of L_{ads} between the Connolly surfaces. The adsorbed molecule can then interact with pore surfaces at its opposite sides, giving a higher heat of adsorption, that is, higher affinity. In addition, the "intrinsic" porosity of SCA adds to the "extrinsic" porosity associated with the newly created surfaces from the introduction of the SCA molecules into MIL-101 (Scheme 1).

The adsorptive characteristics of the SCA@MIL-101 composites were further probed with CO_2 and CH_4 as adsorbates up to pressures of 1 bar. The SCA@MIL-101-*w* ($w = 5$, 10, 30) composites demonstrated 71.0, 83.8, and 102.9 cm^3 g^{-1} uptakes of CO_2 at 1 bar and 273 K, which is in all cases larger than that observed for MIL-101 (65.8 cm^3 g^{-1}) at 1 bar. An advantage is also retained at 293 K, despite the much lower surface areas of the SCA@MIL-101 composites (Fig. 3c, d and S11†). The low-pressure part of the CO_2 adsorption isotherm for MOF materials usually has a low-slope curvature, with a slope well approximating the Henry constant (tending to the exact Henry value with the pressure tending to zero). Accordingly, the higher affinity of all the MIL-101 based composites compared to that of MIL-101 – which was one of the objectives of the work – is manifested in the higher tangent slope of the respective adsorption isotherms (Fig. 3c, d, S12, S13 and Table S4†).

According to the expectations, the higher affinity of MIL-101 based composites is associated with the smaller space-partitioned pores, which interact more strongly with the adsorbate but have a relatively small volume. At pressures higher than ~1 bar, the uptake for MIL-101 quickly surpasses that for SCA@MIL-101-30 in terms of CO_2 adsorption as was demonstrated using an adsorption isotherm up to 20 bar and 293 K (Fig. S14†). The primary objective regarding the SCA@MIL-101-30 composite is to ensure high affinities at low pressures, which is a criterion for CO_2 separation from, for example, flue gases. From the virial analysis of the CO_2 adsorption measurements at 273 and 293 K the heat of adsorption (Q_{st}) of CO_2 and the effect of the pore space partition can be quantified (Fig. 4a and S15–S18†). Interestingly, the heat of adsorption values for MIL-101 near zero coverage, $Q_{st}^0 =$ 48 kJ mol^{-1} as well as at very low loadings are higher than the respective values for the composites, 33, 37, and 42 kJ mol^{-1} for $w = 5$, 10, 30. The lower Q_{st}^0 for the composites *vs.* MIL-101 can

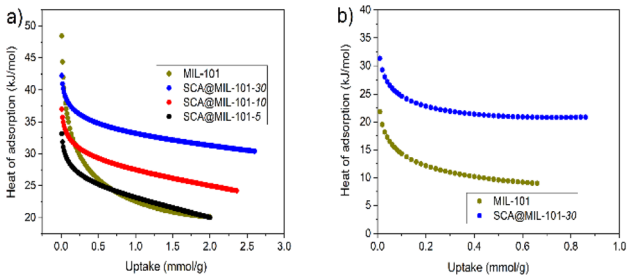

Fig. 4 (a) Isosteric heats of adsorption, Q_{st}, of CO_2 for MIL-101 and the derived SCA@MIL-101 composites from Freundlich–Langmuir fitting of 273 K and 293 K isotherms (*cf.* Fig. S12 and S13†) and (b) isosteric heats of adsorption, Q_{st} for CH_4 for the SCA@MIL-101-30 composite and MIL-101 calculated using Freundlich–Langmuir fitting of 273 K and 293 K isotherms (*cf.* Fig. S20†).

be explained through the "sheltering" or blocking of the strongest interactions sites, which are the Cr–OH/OH_2/O_2C sites, through hydrogen bonding from the –OH and –SO_3H groups of the SCA molecules. Hence, these high heat of adsorption Cr–OH/OH_2/O_2C sites are inaccessible for the CO_2 molecules.

However, Q_{st}^0 of the composites increases, as expected, with the loading of SCA. Yet, and importantly, the Q_{st} values for the SCA@MIL-101-10 and -30 composites overcome the values of MIL-101 already at low loadings of 0.25 and 0.13 mmol g^{-1}, respectively. This is due to the set of polar groups in the SCA molecule together with the pore partitioning such that the CO_2 molecule interacts with pore surfaces at its opposite sides, giving a higher heat of adsorption.

The average uptake of CO_2 at ~1 bar for the SCA@MIL-101 composites is generally better than that for other non-amine modified MIL-101 composites, including MWCNT@MIL-101, silica-rich rice husk ash@MIL-101, and activated carbon-MIL-101 hybrids or on par with amine-modified MIL-101 composites (Table S6†). The CO_2 uptake for the composites reported here reaches 4.6 mmol g^{-1} and 2.6 mmol g^{-1} (17 wt% and 10 wt% at 273 K and 293 K, respectively) for SCA@MIL-101-30 at 1 bar which is somewhat better than that for CB6@MIL-101, where CB6 is a cucurbit[6]uril which contains N atoms.[22] For comparison, MIL-101(Cr)–NH_2 with the 2-amino-benzene-1,4-dicarboxylate linker achieves a CO_2 uptake of 5.1 and 3.6 mmol g^{-1} at 273 and 293 K, 1 bar, respectively.[42] The partially (1%) fluorine functionalized MIL-101(Cr)–4F(1%) with the 2,3,5,6-tetrafluoro-benzene-1,4-dicarboxylate linker showed an expectedly higher CO_2 uptake of 19.4, 7.1, and 5.3 mmol g^{-1} (1 bar) at the lower temperatures of 196 K, 212 K, and 231 K.[43] The average affinity expressed as uptake at 1 bar is, however, a weak indicator of the efficiency of gas separation at (much) lower than atmospheric partial pressures, which are typical for real world applications. Hence, an estimation of the real-world gas separation efficiency is desirable.

The ideal adsorbed solution theory (IAST) was applied to the collected adsorption data to estimate the CO_2/N_2 selectivities of the materials at 293 K (Fig. S19†). The IAST selectivity values for MIL-101 and SCA@MIL-101-w (w = 5, 10, 30) were determined to 4, 8, 10, and 11 at 293 K and 1 bar, respectively, for a flue gas modeling 15 : 85 v : v CO_2/N_2 gas mixture (Table S5†). The CO_2/N_2 selectivity increases with SCA loading, with the molar fraction of CO_2 and with the lower absolute pressure (Fig. S19b†). For comparison, the CO_2/N_2 adsorption selectivity for MIL-101(Cr)–NH_2 was 73 at 273 K (100 at 293 K), estimated from the ratios of the adsorption isotherm slopes at 273 K and 293 K.[42] For MIL-101(Cr)–4F(1%) a $CO_2 : N_2$ selectivity of 22 was estimated from the diffusion time constants for CO_2 at 0.15 bar and N_2 at 0.75 bar at 313 K.[43] The current work aimed to use the "pore-partitioning effect", *i.e.* the decrease of the pore-sizes in the large cavities of MIL-101 to make them optimally commensurate with the size of the adsorbate, in this case, CO_2. The incorporation of SCA molecules creates new surfaces, including the ones associated with their intrinsic porosity. The incorporation allows for an increase in the relative affinity towards CO_2 compared to N_2, as the former, being much more polarizable, forms enhanced vdW contacts, particularly with polar groups, such as OH or SO_3H. This increased affinity could be seen in all SCA@MIL materials, confirming the pore-partitioning approach. These results showed that the IAST values increased by increasing the content of incorporated SCA molecules which was the main purpose of the present study.

The SCA@MIL-101-30 composite demonstrated an uptake of 1.5 mmol g^{-1} CH_4 at 1 bar and 273 K, which is higher than that observed for MIL-101 (1.1 mmol g^{-1}) at 1 bar. Same as for the CO_2 uptake, a higher value was obtained for the SCA@MIL-101-30 composite at 293 K, even though the composite showed much lower surface areas (Fig. S20 and Table S6†). Despite the higher uptakes at both 273 and 293 K for SCA@MIL-101-30, the difference in uptake is only around ~30% which is comparable to the CO_2 uptake. This higher uptake could be related to the smaller partitioned pore space which enables increased surface interactions with the adsorbate as in the CO_2 case.

From the virial analysis of the CH_4 adsorption measurements at 273 and 293 K the effect of the pore space partition and the Q_{st} value of CH_4 can be obtained (Fig. 4b, S21 and S22†). SCA@MIL-101-30 showed significantly higher Q_{st}^0 values (31 kJ mol^{-1}) than neat MIL-101 (22 kJ mol^{-1}). CH_4 does not need the polar high-energy binding sites in MIL-101 as CO_2 does and were occupied by SCA (see above). Instead, CH_4 binds to the hydrophobic aromatic-ring sites through C–H$\cdots\pi$ interactions. The incorporation of SCA added the possibility for such C–H$\cdots\pi$ interactions through its aromatic segment.

The CH_4 uptake and the CH_4/N_2 selectivity for SCA@MIL-30 were compared to the respective values for MIL-101 (Fig. S23 and S24†). The molar uptake of CH_4 at 1 bar and 273 K is ~50% higher than that of N_2 for MIL-101, and slightly more than twice for SCA@MIL-30. Besides, the N_2 uptake is nearly the same for both materials with a slight advantage for MIL-101. The two observations above show that the pore-partitioning incorporation of the SCA molecules is more beneficial for CH_4 uptake than for the N_2 uptake to participate in weak vdW interactions. The relative affinity of SCA@MIL-101-30 for CH_4 is higher than that of MIL-101. The CH_4/N_2 IAST selectivity values for MIL-101 and SCA@MIL-101-30 were determined at 25 vol% CH_4 and 273 K to be 1.3 and 2.1, respectively (Fig. S24†). Thus, the SCA@MIL-101-30 composite exhibited better selectivity regarding a CH_4/

N_2 gas mixture than MIL-101 which is attributed to the smaller pores of the composite.

Finally, the CO_2 and CH_4 selectivities manifested by both SCA@MIL-101-30 and MIL-101 are interesting subjects for comparison (Fig. S25 and S26†). The higher affinity of CO_2 compared to CH_4 is evidently expected, as the more polarizable CO_2 tends to form stronger vdW interactions compared to CH_4. Thus, the SCA@MIL-101-30 composite showed a higher CO_2/CH_4 IAST selectivity of ~6 at 25 vol% CO_2 compared to MIL-101, with 4 (Table S5†). This result reflects the higher increase towards CO_2 affinity for the SCA@MIL-101-30 compared to MIL-101, thereby increasing the selectivity in this particular case.

6. Catalytic activity of SCA@MIL-101 in the esterification of carboxylic acids

The SCA molecule and MIL-101 serve as potent Brønsted-acidic catalysts.[44,45] To assess the synergistic effect of SCA and MIL-101, SCA@MIL-101-30 was tested as a catalyst in the formation of carboxylic acid esters, taking into account the industrial significance of biofuel production, and the relevance of this reaction for testing both the effective acidity and accessibility of the active sites using different substrates.

SCA@MIL-101-30 was activated before it was used or reused and the general method of performing the catalytic experiments is given in the experimental section (ESI Section 3.3; see also Fig. S29†). For comparison, H_2SO_4 as a homogeneous catalyst was used and MIL-101 as a heterogeneous one (Table 2), and the reaction was monitored by GC/MS. The standard reaction time was adjusted in such a way, that the synthesis using H_2SO_4 should give a quantitative conversion in the esterification of benzoic acid by methanol. Under these conditions the SCA@MIL-101-30 composite demonstrated also a near quantitative conversion of ~98%, while the conversions using a comparative amount of SCA or MIL-101 alone ensured only ~50% and ~20% conversions, respectively (Table 2). The conversion was less than 5% when no catalyst was used. The esterification mechanism involves the activation of the carboxylic acid by protonation of the carboxyl group with a subsequent attack of the alcohol nucleophile.[46]

Both non-branched carboxylic acids and non-branched alcohols can pass through the pores since the size of their smallest projections is comparable to the size of an N_2 molecule (*e.g.*, the kinetic diameter of MeOH is approx. 3.6 Å), and the respective ester product is also comparable. Table 3 summarizes the esterification reactions. The reusability of the SCA@MIL-101-30 catalyst was tested for recycling *via* its recovery by centrifugation, washing, and pre-drying after each reaction (see the ESI†). The repeated catalytic cycles showed only a small drop in conversion under the same conditions (Fig. 5). The retained efficiency not only confirms the stability of the catalyst but also indirectly corroborates the low leaching of SCA from the composite.

Table 2 Esterification reaction of benzoic acid with methanol[a]

Time (h)	Temp. (°C)	Catalyst	% conversion[b]
4	120	20 mg SCA@MIL-101-30	>98
		20 mg MIL-101	~20
		150 μL of H_2SO_4	100
		20 mg of SCA	~50
		No catalyst	<5

[a] Benzoic acid 1.0 mmol, methanol 6.0 mmol. [b] With respect to benzoic acid.

Table 3 Esterification of carboxylic acids by alcohols using the SCA@MIL-101-30 composite as a catalyst[a]

Substrate	Nucleophile	% conversion[b]
Benzoic acid	MeOH	>99
	EtOH	>98
	n-Propanol	>80
Acetic acid	MeOH	>99
	EtOH	>99
	n-Propanol	>98
Phthalic acid	MeOH	>99
	EtOH	>95
	n-Propanol	>99
Pivalic acid	MeOH	>99
	EtOH	>95
	n-Propanol	>96

[a] All reactions were carried out under the same conditions: 4 h, 120 °C, acid 1.0 mmol, alcohol 6.0 mmol and with 20.0 mg of the SCA@MIL-101-30 catalyst. [b] With respect to the carboxylic acid.

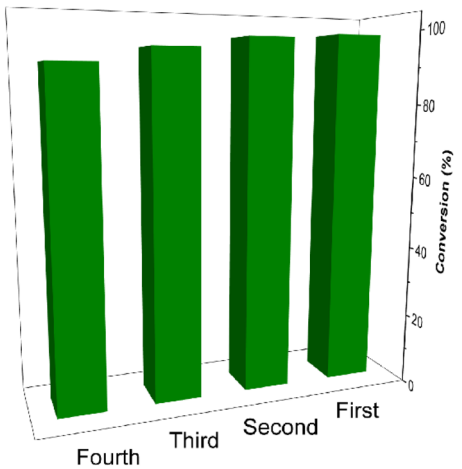

Fig. 5 The observed conversions in the repeated catalytic cycles of the esterification of benzoic acid using the initial (first) and recovered SCA@MIL-101-30 composites.

7. Conclusion

The incorporation of SCA with dimensions slightly smaller than the largest pore opening of MIL-101 was successfully achieved by adsorptive loading. The SCA@MIL-101 composites were intended to be developed for "locking-in" the SCA molecules for their further modification. However, the SCA@MIL-101 composites, which were unambiguously verified by PXRD,

SEM/EDX, TEM, TGA, IR and digestion ^{1}H NMR analysis were found to be stable, with a very low tendency towards SCA leaching, which made them an interesting target themselves.

The maximum reached SCA loading of 30 wt% in SCA@MIL-101-30, when a high excess of a concentrated SCA solution was used during the loading, is lower than the >1 g g^{-1} reached by other guests, including ones with significant size. The adsorption by the smaller MIL-101 cages is hindered, due to the smaller size of their entrance pore window than the size of the SCA molecule. The maximal achievable loading did not lead to pore-clogging, retaining 1073 m^2 g^{-1} of the BET surface area compared to 2658 m^2 g^{-1} for MIL-101.

The adsorption characteristics of SCA@MIL-101 show a significant affinity enhancement towards both CO_2 and CH_4 at <1 bar pressures compared to MIL-101 in terms of CO_2 and CH_4 uptake and heat of adsorption with increasing uptake. This proves the utility of the "pore-space partitioning" approach *via* the incorporation of the semi-rigid bowl-shaped SCA molecules, providing smaller pores with higher affinities towards the small adsorbate molecules. This has to be judged against the much lower surface area (see above) and pore volume for $w = 30$ wt% SCA in MIL-101 ($V_{pore} = 0.52$ cm^3 g^{-1}) *vs.* neat MIL-101 (1.0 cm^3 g^{-1}) and is contrary to the impression, which is often given in the MOF literature, that large surface area and large pore volume are better for MOFs. Instead, a pore size design which is achieved here through pore partitioning can be a better option.[47] As the SCA molecule has both polar and non-polar parts, the enhancement is reached for both CO_2 and CH_4 as well as in their IAST selectivities regarding CO_2/N_2 and CO_2/CH_4 compared to MIL-101, but not in the case of CH_4/N_2 selectivities, where the relative affinity gains for both gases are comparable and hence compensated.

It was found that the retained accessibility of the pores even at the highest loading for small substrates renders SCA@MIL-101-30 a potent Brønsted acid catalyst in the reaction of carboxylic acid esterification by alcohols. The composite acts much better than MIL-101 and is on par with H_2SO_4 under the chosen conditions. Importantly, the small decrease of catalytic activity in the repeated cycles proves the relatively low leaching, evidently due to the high affinity of the framework pores towards SCA. The SCA@MIL-101 composites with the already functional and further functionalizable semi-rigid bowl-shaped tetrasulfocalix[4]arene possessing intrinsic porosity (allowing them to also function as hosts) represent a step forward compared to the rigid, but non-functionalizable cucurbiturils, which already have shown excellent possibilities regarding the pore space partitioning approach. The further functionalization of the calixarene in the SCA@MIL-101 composite opens possibilities for the synthesis of well-defined secondary@primary host composites with practically negligible leakage and with a full elucidation of the host@MOF synergy in selective adsorption and separation of small molecules, as well as catalysis.

Data availability

The data supporting this article have been included as part of the ESI.†

Author contributions

Saied Shafiei Navid: investigation, methodology, writing – original draft. Robert Oestreich: methodology. Soheil Abdpour: methodology. Thi Hai Yen Beglau: methodology. Rahman Hosseinzadeh: conceptualization, supervision, writing – review & editing. Christoph Janiak: conceptualization, supervision, writing – review & editing.

Conflicts of interest

There are no conflicts to declare.

Acknowledgements

The authors acknowledge the funding from the Research Council of the University of Mazandaran and the internal funds of Heinrich Heine University Düsseldorf (further referred to as HHU). The authors thank Dr István Boldog (HHU) for delineating the project and adjusting the concept of this paper to be conformant with a larger research project; for the preparation of the molecular graphics; for providing the methods for calculation of the SCA content; and for rewriting of the whole manuscript with reformulating the key points to be conformant to standard demands. Mr Marcus Fetzer (HHU) is acknowledged for his consultative help in carrying out the synthetic work, Mr Lars Rademacher for methodology, and Ms Birgit Tommes for measuring the IR spectra. The research was funded in part by the Deutsche Forschungsgemeinschaft (DFG) within the Priority Program SPP 1928/2 COORNETs (grant Ja466/43-1).

References

1 A. G. Slater and A. I. Cooper, *Science*, 2015, **348**, aaa8075, DOI: **10.1126/science.aaa8075**.
2 J. Liang, A. Nuhnen, S. Millan, H. Breitzke, V. Gvilava, G. Buntkowsky and C. Janiak, *Angew. Chem., Int. Ed.*, 2020, **59**, 6068–6073, DOI: **10.1002/anie.201916002**.
3 J. Caro, *Curr. Opin. Chem. Eng.*, 2011, **1**, 77–83, DOI: **10.1016/j.coche.2011.08.007**.
4 C. C. Hou and Q. Xu, *Adv. Energy Mater.*, 2019, **9**, 1801307, DOI: **10.1002/aenm.201801307**.
5 R. Freund, O. Zaremba, G. Arnauts, R. Ameloot, G. Skorupskii, M. Dincă, A. Bavykina, J. Gascon, A. Ejsmont and J. Goscianska, *Angew. Chem., Int. Ed.*, 2021, **60**, 23975–24001, DOI: **10.1002/anie.202106259**.
6 G. Zhang, O. Presly, F. White, I. M. Oppel and M. Mastalerz, *Angew. Chem., Int. Ed.*, 2014, **53**, 1516–1520, DOI: **10.1002/anie.201308924**.
7 I. Pyka, D. Lubczyk, M. D. S. Saiju, J. Salbeck and S. R. Waldvogel, *ChemPlusChem*, 2017, **82**, 1116–1120, DOI: **10.1002/cplu.201600583**.
8 A. N. Hong, H. Yang, X. Bu and P. Feng, *EnergyChem*, 2022, **4**, 100080, DOI: **10.1016/j.enchem.2022.100080**.
9 Q. G. Zhai, X. Bu, X. Zhao, D. S. Li and P. Feng, *Acc. Chem. Res.*, 2017, **50**, 407–417, DOI: **10.1021/acs.accounts.6b00526**.

10 T. Zhou, S. Liu, E. V. Alexandrov, H. Guo, P. Gao, S. Mi, Q. Su, X. Guo and T. Hu, *Cryst. Growth Des.*, 2021, **21**, 5724–5730, DOI: **10.1021/acs.cgd.1c00564**.
11 T. Rajkumar, D. Kukkar, K. H. Kim, J. R. Sohn and A. Deep, *J. Ind. Eng. Chem.*, 2019, **72**, 50–66, DOI: **10.1016/j.jiec.2018.12.048**.
12 Y. Sun, J. Liang, P. Brandt, A. Spieß, S. Öztürk and C. Janiak, *Nanoscale*, 2021, **13**, 15952–15962, DOI: **10.1039/D1NR04432J**.
13 G. Férey, C. Mellot-Draznieks, C. Serre, F. Millange, J. Dutour, S. Surblé and I. Margiolaki, *Science*, 2005, **309**, 2040–2042, DOI: **10.1126/science.1116275**.
14 T. K. Trung, N. A. Ramsahye, P. Trens, N. Tanchoux, C. Serre, F. Fajula and G. Férey, *Microporous Mesoporous Mater.*, 2010, **134**, 134–140, DOI: **10.1016/j.micromeso.2010.05.018**.
15 A. P. Demchenko, Recognition Units Built of Small Macrocyclic Molecules, in *Introduction to Fluorescence Sensing*, Springer, Cham., 2023, vol. 2, pp. 73–102, DOI: **10.1007/978-3-031-19089-6_3**.
16 M. De Rosa, P. La Manna, C. Talotta, A. Soriente, C. Gaeta and P. Neri, *Front. Chem.*, 2018, **6**, 84, DOI: **10.3389/fchem.2018.00084**.
17 A. Chaix, G. Mouchaham, A. Shkurenko, P. Hoang, B. Moosa, P. M. Bhatt, K. Adil, K. N. Salama, M. Eddaoudi and N. M. Khashab, *J. Am. Chem. Soc.*, 2018, **140**, 14571–14575, DOI: **10.1021/jacs.8b08770**.
18 S. Shafiei-Navid, R. Hosseinzadeh and M. Ghani, *Microchem. J.*, 2022, **183**, 107985, DOI: **10.1016/j.microc.2022.107985**.
19 Y. Tu, G. Xu, L. Jiang, X. Hu, J. Xu, X. Xie and A. Li, *Chem. Eng. J.*, 2020, **382**, 123015, DOI: **10.1016/j.cej.2019.123015**.
20 H. Moll, K. M. Alenezi, A. O. Alshammari, A. Haque, J. Humaidi, R. Soury, E. Azzam, F. Abdulaziz, S. Latif and M. Vraneš, *J. Chem. Soc. Pak.*, 2023, **45**, 113, DOI: **10.52568/001216/jcsp/45.02.2023**.
21 X. Zhang, S. Tong, J. Zhu and M. X. Wang, *Chem. Sci.*, 2023, **14**, 827–832, DOI: **10.1039/D2SC06234H**.
22 J. Liang, V. Gvilava, C. Jansen, S. Öztürk, A. Spieß, J. Lin, S. Xing, Y. Sun, H. Wang and C. Janiak, *Angew. Chem., Int. Ed.*, 2021, **60**, 15365–15370, DOI: **10.1002/anie.202100675**.
23 Q. Wu, J. Liang, D. Wang, R. Wang and C. Janiak, *Chem. Soc. Rev.*, 2025, DOI: **10.1039/d4cs00371c**, in press.
24 S. Krajangsri, N. Muangsin and B. Pulpoka, *J. Inclusion Phenom. Macrocyclic Chem.*, 2021, **101**, 195–204, DOI: **10.1007/s10847-021-01091-5**.
25 S. Chen, Q. Chen, S. Dong, J. Ma, Y. W. Yang, L. Chen and H. Gao, *Macromol. Biosci.*, 2018, **18**, 1800317, DOI: **10.1002/mabi.201800317**.
26 M. Peng, A. M. Kaczmarek and K. V. Hecke, *ACS Appl. Mater. Interfaces*, 2022, **14**, 14367–14379, DOI: **10.1021/acsami.2c01332**.
27 M. Yamada and F. Hamada, *CrystEngComm*, 2011, **13**, 2494–2499, DOI: **10.1039/C0CE00824A**.
28 R. Vargas, J. Garza, A. Martínez and I. A. Ibarra, *Chem. Commun.*, 2024, **60**, 3008–3018, DOI: **10.1039/d3cc06347j**.
29 V. d. C. Cotlame-Salinas, A. López-Olvera, A. Islas-Jácome, E. González-Zamora and I. A. Ibarra, *React. Chem. Eng.*, 2021, **6**, 441–453, DOI: **10.1039/d0re00410c**.
30 Y. K. Agrawal, J. P. Pancholi and J. M. Vyas, *J. Sci. Ind. Res.*, 2009, **68**, 745–768, **https://nopr.niscpr.res.in/bitstream/123456789/5949/1/JSIR68(9)745-768.pdf**.
31 M. Nemati, R. Hosseinzadeh and M. Mohadjerani, *Spectrochim. Acta, Part A*, 2021, **245**, 118950, DOI: **10.1016/j.saa.2020.118950**.
32 L. Eddaif, A. Shaban and J. Telegdi, *Int. J. Environ. Anal. Chem.*, 2019, **99**, 824–853, DOI: **10.1080/03067319.2019.1616708**.
33 C. D. Gutsche, I. Alam, M. Iqbal, T. Mangiafico, K. C. Nam, J. Rogers and K. A. See, *J. Inclusion Phenom. Mol. Recognit. Chem.*, 1989, **7**, 61–72, DOI: **10.1007/BF01112783**.
34 A. Mazinani, K. Zare, O. Moradi and H. Attar, *Chemosphere*, 2022, **299**, 134459, DOI: **10.1016/j.chemosphere.2022.134459**.
35 L. Tian, S. Zhou, J. Zhao, Q. Xu, N. Li, D. Chen, H. Li, J. He and J. Lu, *J. Hazard. Mater.*, 2023, **441**, 129873, DOI: **10.1016/j.jhazmat.2022.129873**.
36 M. Rahimi, R. Karimian, E. Mostafidi, E. Noruzi, S. Taghizadeh, B. Shokouhi and H. Samadi Kafil, *New J. Chem.*, 2018, **42**, 13010–13024, DOI: **10.1039/C8NJ01790E**.
37 D. L. Silva, S. A. Fernandes, A. A. Sabino and Â. Fátima, *Tetrahedron Lett.*, 2011, **52**, 6328–6330, DOI: **10.1016/j.tetlet.2011.08.175**.
38 M. Zou, M. Dong and T. Zhao, *Int. J. Mol. Sci.*, 2022, **23**, 9396, DOI: **10.3390/ijms23169396**.
39 Y. Tauran, A. Brioude, P. Shahgaldian, A. Cumbo, B. Kim, F. Perret, A. W. Coleman and I. Montasser, *Chem. Commun.*, 2012, **48**, 9483–9485, DOI: **10.1039/C2CC34670B**.
40 T. Zhao, F. Jeremias, I. Boldog, B. Nguyen, S. K. Henninger and C. Janiak, *Dalton Trans.*, 2015, **44**, 16791–16801, DOI: **10.1039/C5DT02625C**.
41 V. L. Furer, A. E. Vandyukov, A. R. Khamatgalimov, S. R. Kleshnina, S. E. Solovieva, I. S. Antipin and V. I. Kovalenko, *J. Mol. Struct.*, 2019, **1195**, 403–410, DOI: **10.1016/j.molstruc.2019.06.008**.
42 A. Khutia and C. Janiak, *Dalton Trans.*, 2014, **43**, 1338–1347, DOI: **10.1039/c3dt52365a**.
43 M. L. Díaz-Ramírez, E. Sánchez-González, J. R. Álvarez, G. A. González-Martínez, S. Horike, K. Kadota, K. Sumida, E. González-Zamora, M.-A. Springuel-Huet, A. Gutiérrez-Alejandre, V. Jancik, S. Furukawa, S. Kitagawa, I. A. Ibarra and E. Lima, *J. Mater. Chem. A*, 2019, **7**, 15101–15112, DOI: **10.1039/c9ta02237f**.
44 A. Herbst and C. Janiak, *New J. Chem.*, 2016, **40**, 7958–7967, DOI: **10.1039/C6NJ01399F**.
45 A. Herbst and C. Janiak, *CrystEngComm*, 2017, **19**, 4092–4117, DOI: **10.1039/C6CE01782G**.
46 Y. Dou, H. Zhang, A. Zhou, F. Yang, L. Shu, Y. She and J. R. Li, *Ind. Eng. Chem. Res.*, 2018, **57**, 8388–8395, DOI: **10.1021/acs.iecr.8b01239**.
47 S. Xing, J. Liang, P. Brandt, F. Schäfer, A. Nuhnen, T. Heinen, I. Boldog, J. Möllmer, M. Lange, O. Weingart and C. Janiak, *Angew. Chem., Int. Ed.*, 2021, **60**, 17998–18005, DOI: **10.1002/anie.202105229**.

